Authors for correspondence:
Diana D. Chin
e-mail: ddchin@alumni.stanford.edu
David Lentink
e-mail: d.lentink@rug.nl

THE ROYAL SOCIETY PUBLISHING

Birds both avoid and control collisions by harnessing visually guided force vectoring

Diana D. Chin[1] and David Lentink[1,2]

[1]Department of Mechanical Engineering, Stanford University, Stanford, CA, USA
[2]Faculty of Science and Engineering, University of Groningen, Groningen, Groningen, The Netherlands

DDC, 0000-0002-3015-7645; DL, 0000-0003-4717-6815

Birds frequently manoeuvre around plant clutter in complex-structured habitats. To understand how they rapidly negotiate obstacles while flying between branches, we measured how foraging Pacific parrotlets avoid horizontal strings obstructing their preferred flight path. Informed by visual cues, the birds redirect forces with their legs and wings to manoeuvre around the obstacle and make a controlled collision with the goal perch. The birds accomplish aerodynamic force vectoring by adjusting their body pitch, stroke plane angle and lift-to-drag ratios beat-by-beat, resulting in a range of about 100° relative to the horizontal plane. The key role of drag in force vectoring revises earlier ideas on how the avian stroke plane and body angle correspond to aerodynamic force direction—providing new mechanistic insight into avian manoeuvring—and how the evolution of flight may have relied on harnessing drag.

1. Introduction

Foraging birds, bats and insects frequently navigate cluttered habitats, negotiating obstacles on the wing. The severity of a collision depends largely on an animal's momentum (mass times velocity) during impact [1], so it is critical for larger animals like birds and bats to use rapid changes in posture [2,3] or reliable manoeuvring strategies to avoid injury. Arboreal birds, in particular, are adept at negotiating intervening branches as they perform short flights (less than 1 m) up to 30 times per minute [4] in search of food. These rapid manoeuvres require them to redirect both terrestrial forces exerted by their legs during take-off and landing as well as aerodynamic forces exerted by their wings. However, the mechanisms that enable this redirection of forces in the global frame—what we refer to as 'force vectoring'—are not well understood [5].

Our current understanding of manoeuvring animal flight comes mostly from studies on turning flights made by insects [6–8], bats [9] and birds [10,11] in uncluttered airspace. These animals often perform rolling banked turns to redirect aerodynamic forces [6,9,10,12,13], a strategy that has been likened to that of helicopters rolling into turns [10,14,15]. In addition to rolling, insects [7,8,16] and hummingbirds [17,18] can also rely on stroke plane angle and other wingbeat kinematics adjustments to turn without adjusting their body orientation. Prior studies have shown how insects [16], hummingbirds [19] and small bats [9] perform tighter turns compared with generalist birds. It is, therefore, unclear to what extent generalist birds redirect forces like these smaller animals.

Furthermore, different aerodynamic force vectoring strategies, such as pitching instead of yawing or rolling, are probably required to avoid horizontal obstacles. The importance of pitching manoeuvres also extends beyond obstacle avoidance. Juvenile birds exhibit an approximately 30° range in body pitch orientation when performing the fundamental avian wing-stroke, which is believed to have been established for aerodynamic function early in the evolution of flight [20]. Birds can also use pitching movements to accelerate after take-off and brake for landing [21–23]. However, the extent to which aerodynamic forces are redirected in the global frame by these pitching

manoeuvres, or even by yawing and rolling, is not fully understood. Aerodynamic force vectoring in birds has only been derived from combining mass distribution and kinematics measurements [10,11,18,24], and has never been measured directly in a freely flying animal *in vivo*.

To quantify the strategies and mechanisms involved in their force vectoring, we studied how five Pacific parrotlets (*Forpus coelestis*; $N = 5$), generalist arboreal birds [25], navigated around horizontal aerial obstacles while flying voluntarily between perches to forage seeds. We filmed their manoeuvres at high speed while they flew in a two-dimensional aerodynamic force platform (AFP; see Material and methods). This custom set-up enabled us to non-intrusively measure both terrestrial forces (using instrumented perches) and aerial horizontal and vertical forces *in vivo*. We compared flights without obstacles, the baseline, with flights in which birds negotiated horizontal strings that spanned the full width of the AFP. To evaluate if and how the proximity of the obstacle to the take-off or landing perch would affect their flight strategy, the strings were positioned at 25, 40 or 55 cm from the take-off perch (figure 1*a*).

2. Results

2.1. Flight behaviour and impulse redirection

Parrotlets effectively redirect terrestrial and aerodynamic forces (relative to the global frame) to reach their goal perch when it is blocked by an aerial obstacle (figure 1*a*). Initial wingbeat impulses after take-off are consistent spatially (figure 1*b*) and temporally for most flight variations (electronic supplementary material, figure S1). By contrast, wingbeat impulses later in each flight exhibit visibly more scatter, particularly when flying over obstacles and under the 55 cm obstacle, which is closest to the goal perch (figure 1*b*; electronic supplementary material, figure S1). Forces generated by their legs and wings during these flights are primarily oriented upwards to support bodyweight and thus overcome gravity (figures 1*c* and 2*a*). However, an additional net impulse (stroke-averaged total force minus bodyweight) is needed to navigate around obstacles between the take-off and goal perches. The reorientation of the take-off leg impulse (figure 2*b*, insets) aligns with the direction taken to avoid the obstacle; take-off impulse is oriented more vertically for a flight over an obstacle, and more horizontally for a flight under an obstacle. These differences are more pronounced when the obstacle is closer to the take-off perch (difference between flying over or under a '25 cm' obstacle = $70 \pm 26°$, '40 cm' = $39 \pm 32°$, '55 cm' = $24 \pm 23°$). The net wingbeat impulse is also redirected beat-by-beat; it is initially oriented more forwards and rotates backwards more consistently when flying under the obstacle (figure 2*b*).

### 2.2. Lift and drag use and reorientation

We combined our force and kinematic measurements to resolve the relative lift (force component acting perpendicular to the wing velocity) and drag (force component acting parallel and opposite to the wing velocity) contributions to the 1775 recorded wingbeats during manoeuvring flights (see Material and methods). We find that higher lift-to-drag ratios are used during flights under an obstacle, particularly after passing the obstacle and for landing (figures 2*a*

and 3*h*). The net forces (total – weight) used for manoeuvring around an obstacle, and for braking before landing, involve more drag (figure 2*b*). Although lift is commonly associated with vertical weight support and drag for horizontal braking force, we find that stroke-averaged lift and drag are frequently repurposed during these flights. During take-off, drag and lift can support weight equivalently—drag contributes up to 55% weight support during obstacle-free flight, and up to 70% upon take-off for flights under the obstacle. Near an obstacle, drag continues to provide up to 50% weight support, and then during landing lift provides up to 40% of the total horizontal braking force. On average, drag contributes more to take-off weight support during flights under an obstacle compared with flights over, particularly when the obstacle is closer to the take-off perch. Similarly, lift contributes more to horizontal braking for flights under an obstacle than for flights over, with more pronounced differences when the obstacle is closer to the goal perch (representative vectors shown in figure 3*a*–*d*; average percentages in electronic supplementary material, table S4). The use of aerodynamic force vectoring as well as lift and drag repurposing is thus adapted to obstacle location. The position of the obstacle drives the ascending and descending flight angles required to manoeuvre around it—showing aerodynamic force vectoring is an essential mechanism that enables birds to perform flights around obstacles.

2.3. Aerodynamic force vectoring mechanism

To achieve aerial force vectoring, birds control both the magnitude and direction of their wingbeat impulse by adjusting their body and wingbeat kinematics as well as lift-to-drag ratios. The total impulse magnitude increases in two cases: after flying over an obstacle during landing, and while flying under an obstacle (figure 3*e*). The average total impulse vector (figure 3*f*) and stroke plane (figure 3*g*), which we directly measured, both rotate forwards to accelerate during take-off and then backwards to brake during landing. The average lift-to-drag ratio ($\overline{L/D}$), which we calculated from measured forces and kinematics (see Material and methods; electronic supplementary material, figure S6), is generally lower flying over the obstacle and higher when flying under (figure 3*h*). To control the wingbeat force magnitude beat-by-beat, the parrotlets modulate their wing velocity (electronic supplementary material, figure S3A) via stroke amplitude (electronic supplementary material, figure S3B) and stroke time (electronic supplementary material, figure S3C). They rely more on reducing downstroke duration, T, than stroke amplitude to increase wing velocity, V, and thus force magnitude; $F \propto V^2 \propto T^{-2}$ (electronic supplementary material, figure S3C).

The parrotlets pitch their bodies as they reorient forces, but the same net impulse direction can be achieved over a range of body angles diverging up to approximately 30° (figure 4*a*), which goes beyond insects [7,8,16] and is on par with predictions from aerodynamic models for manoeuvring hummingbirds [18,26]. In fact, the average direction of a wingbeat impulse relative to the body angle spans a range of over 40° across the different wingbeat types (take-off, before obstacle, after obstacle, or landing; figure 4*b*). By pitching their bodies, the birds also pitch their stroke plane, which remains at a relatively fixed angle with respect to their body angle ($118° \pm 9°$, mean ± s.d.; figure 4*c*). The stroke plane
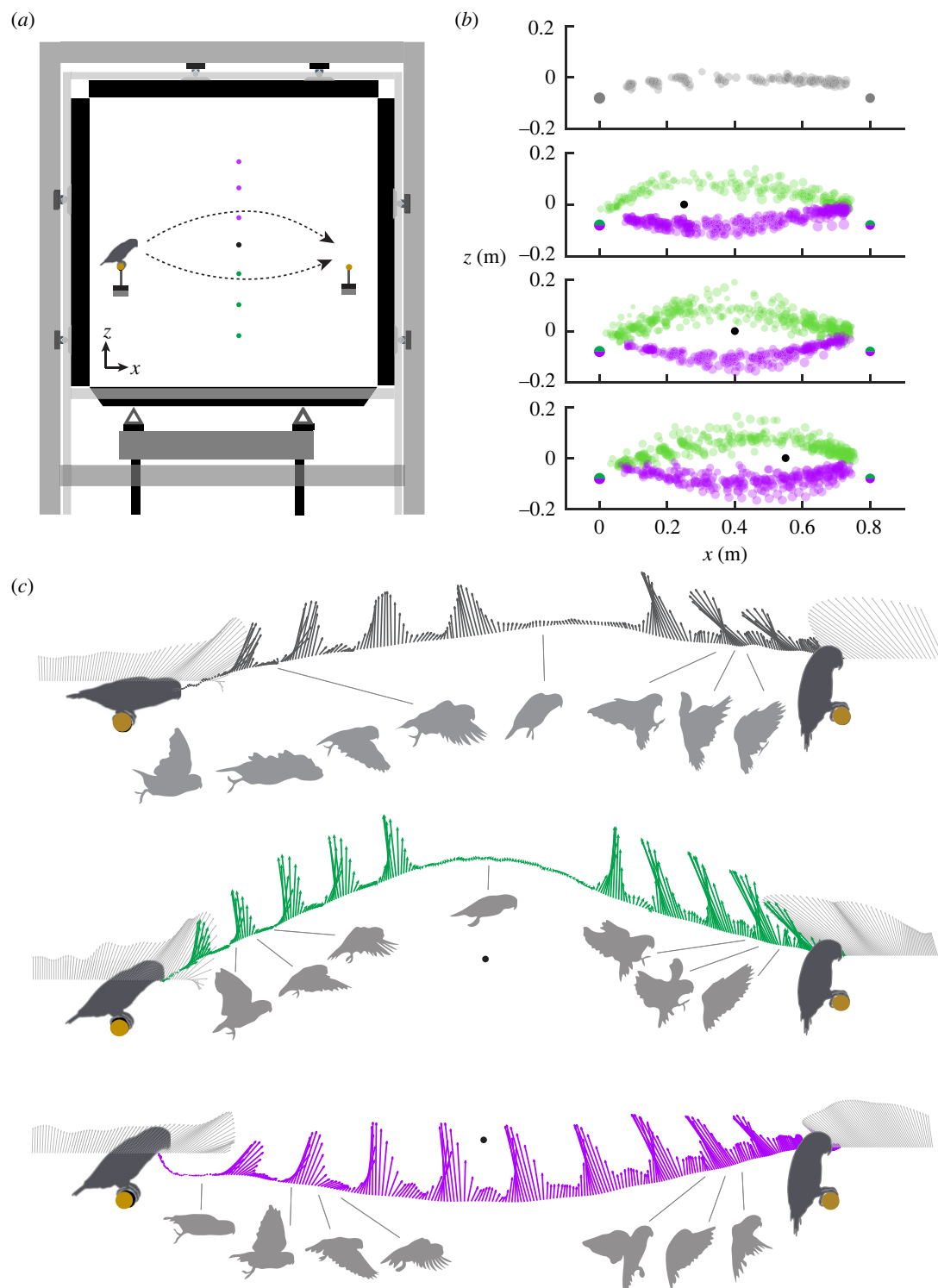
Figure 1. Perch-to-perch flights inside of an AFP quantify the terrestrial and aerodynamic forces that parrotlets generate to negotiate horizontal obstacles. (*a*) We recorded flights between two instrumented perches spaced 80 cm apart in the AFP, both with and without the presence of a horizontal string obstacle (represented by the black circle). The string was positioned at eye-level with the perched bird at distances of 25, 40 and 55 cm from the take-off perch. Additional strings (represented by the purple and green circles) were also added above or below the original so that birds could only fly under or over the obstacle, respectively. Instrumented plates on the top, bottom, front and rear walls of the AFP enable direct measurements of the net vertical and horizontal forces during each flight. (*b*) Mid-downstroke locations across all flights of all five birds show how initial wingbeats are more stereotyped while later wingbeats tend to exhibit more variance, particularly when flying under the 55 cm obstacle. Dot area scales with total impulse. Black dots show obstacle locations and have an area that corresponds to bodyweight impulse during one wingbeat. Net take-off and landing impulses are shown using the same scaling at the corresponding perch locations (only half of the full dot is shown for flights over and under an obstacle). (*c*) Take-off and landing perch forces are shown in light grey, and net aerodynamic forces are shown in dark grey for a representative flight with no string obstacle. Aerodynamic forces are shown in green for a flight over the obstacle, and purple for a flight under the obstacle. The net aerodynamic force vectors are plotted along the trajectory of the bird's eye during each flight.

angle, which we define relative to the global horizontal plane, then largely determines the angle of the net impulse generated by each wingbeat (electronic supplementary material,

figure S4). These relations can be well-approximated by linear functions (figure 4*a,c*; electronic supplementary material, figure S4). We find that the stroke-averaged net
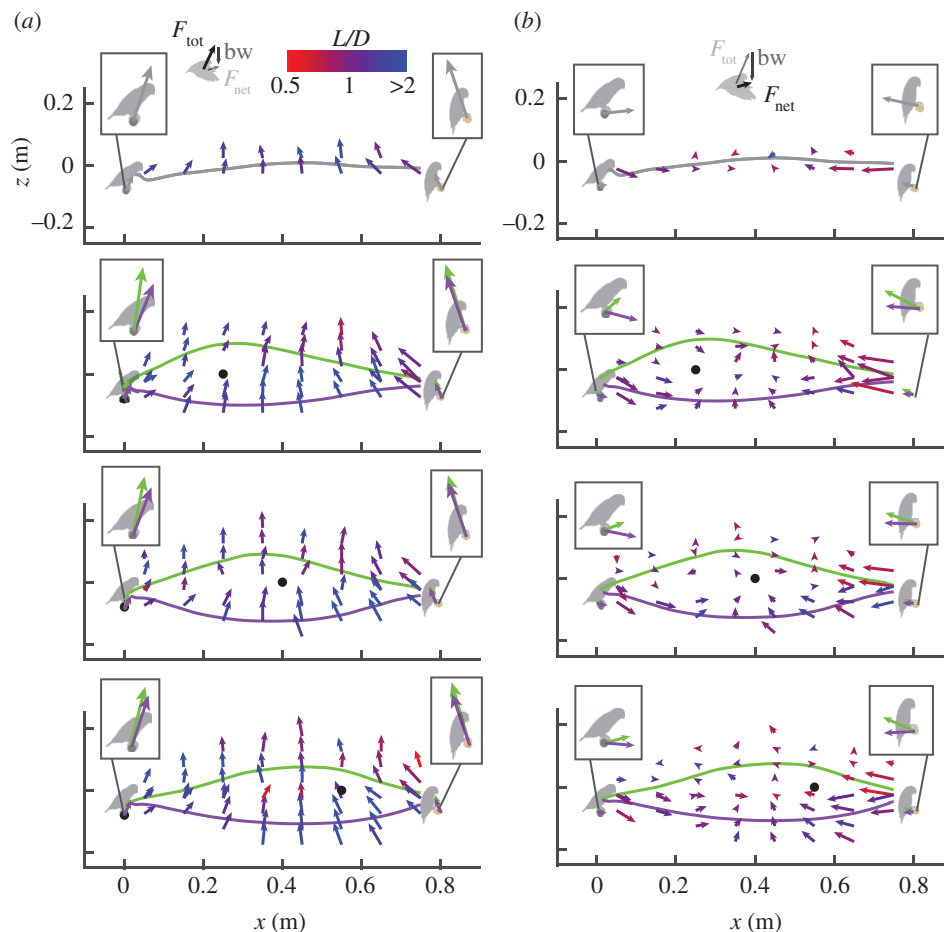
Figure 2. Birds use both terrestrial and aerial force vectoring to negotiate obstacles during foraging flights. (a) Total terrestrial and aerodynamic impulse vectors show how perching forces and wingbeat-averaged forces are mostly used for weight support during these short flights (1 bodyweight impulse is shown by the bw vector in the avatar, and take-off and landing vectors shown in the insets are magnified 3×). Terrestrial impulse vectors show how birds direct impulse from their legs differently to fly over (green) versus under (purple) obstacles during take-off. Impulse vectors from the wings are coloured by relative lift-to-drag (L/D) contributions. Relatively more drag (red) is used before landing, especially when flying over the obstacle, whereas relatively more lift (blue) is used below the obstacle. (b) Net impulse (total minus bodyweight) vectors exhibit clearer differences between flights over versus under an obstacle. The L/D shown in this panel pertains to lift and drag contributions to the net (manoeuvring) forces, and therefore differ from the L/D shown in (a). Differences in the direction of the net take-off impulse from the legs (insets) are most pronounced when the obstacle is closest to the take-off perch (net impulse directions for the 25 cm obstacle: $49° \pm 22°$ (over) versus $-20° \pm 15°$ (under); for the 40 cm obstacle: $24° \pm 31°$ (over) versus $-14° \pm 7°$ (under); for the 55 cm obstacle: $17° \pm 19°$ (over) versus $-7° \pm 13°$ (under)). The same L/D colour scale is shown in both (a) and (b) for comparison, although maximum L/D reaches 3.9 for total forces and 3.4 for net forces (all vectors with L/D > 2 are shown in blue). Impulse averages are pooled across wingbeats from $N = 5$ birds, $n_{baseline} = 20$ flights, $n_{over} = 80$ flights, $n_{under} = 92$ flights on a fixed spatial grid and plotted with their origins at the cell centres (see electronic supplementary material, figure S2). Average flight trajectories are shown in each plot; grey (baseline flights), green (flights over the obstacle) and purple (flights under the obstacle).

impulse is, on average, oriented substantially less than 90° from the stroke plane (figure 4d; electronic supplementary material, figure S4), in contrast to rotorcraft [15] or hovering insects [27]. These diminished angles are explained by the use of more drag; wingbeats with relatively more drag, such as landing wingbeats, exhibit greater deviations from the 90° assumption (figure 4e), because the instantaneous aerodynamic vector angle is $\tan^{-1}(L/D)$ with respect to the stroke direction. The same equation also indicates that at low lift-to-drag ratios—which are typical during take-off, and even more so during manoeuvring and landing when $\overline{L/D}$ is substantially reduced by harnessing drag—the aerodynamic vector angle becomes very sensitive to changes in L/D. This explains why we observe large stroke-averaged force reorientations of up to approximately 50° for $0.5 \lesssim \overline{L/D} \lesssim 2$ (figures 3a–d and 4e). Birds can therefore redirect aerial forces in the global frame—not only by adjusting body and stroke plane angles—but also through variable lift-to-drag ratios.

## 2.4. Time-to-collision guided manoeuvres

To evaluate whether the birds were incorporating visual cues during flight, we measured their head orientation during each wingbeat (see Material and methods). Compared with flights with no obstacle, parrotlets orient their heads more downwards when flying over an obstacle, and more upwards when flying under one (figure 5a,b). By adjusting their head orientation based on the obstacle's location, the birds are able to keep the obstacle within their field of vision, which lies mostly in front and above their head [29], until they pass over or under the obstacle (figure 5c). At the same time, the birds maintain a view of the landing perch throughout the flight (figure 5d). By doing so, they can avoid collisions with the obstacle while controlling their landings according to a visually estimated time-to-collision known as the tau function [30], where tau is equal to the distance to the target divided by the time rate of change of that distance. Here we calculate two
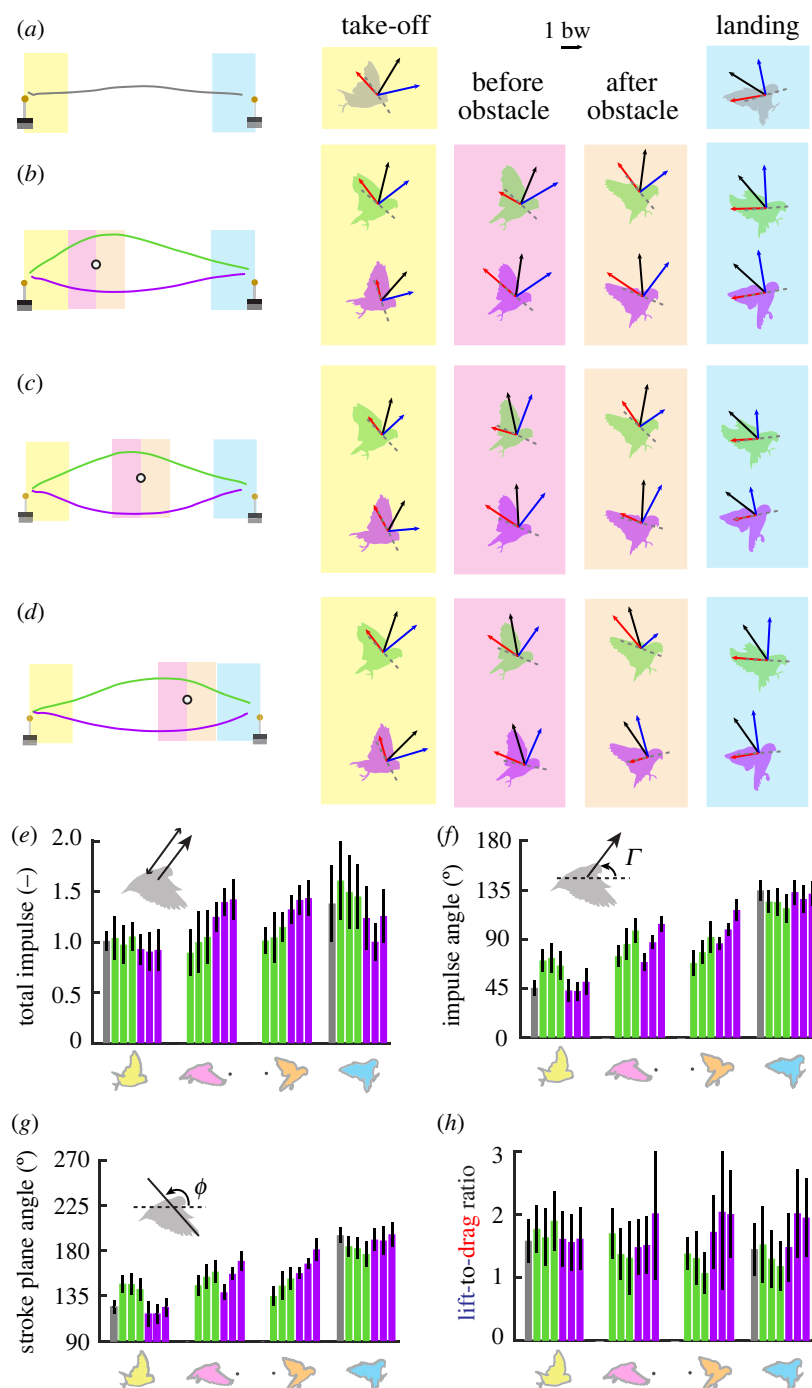
Figure 3. Birds rely on both lift and drag to take off, negotiate obstacles and land. (*a–d*) The lift (blue), drag (red) and net aerodynamic force (black) at mid-downstroke for representative wingbeats are shown for flights with no obstacle (*a*) and flights over and under obstacles placed at 25 cm (*b*), 40 cm (*c*) and 55 cm (*d*). Wingbeat types are based on horizontal proximity to perches and obstacles ('take-off' = less than 15 cm from the take-off perch, 'before obstacle' = less than 10 cm before the obstacle, 'after obstacle' = less than 10 cm past the obstacle, 'landing' = less than 15 cm from the goal perch). Dashed lines show stroke plane angles. Lift and drag components shown are two-dimensional projections of three-dimensional vectors, so they may not appear orthogonal (see Material and methods). Wingbeat-averaged drag contributions to weight support and lift contributions to horizontal braking are summarized in electronic supplementary material table S4. These results are summarized in (*e–h*), which show mean ± s.d. for each variation (from left to right): baseline (if applicable), over 25/40/55 cm, under 25/40/55 cm. (*e*) Total impulse increases during landing wingbeats when flying over an obstacle and during wingbeats near the obstacle when flying under an obstacle (for weight support). Impulses near obstacles tend to increase when the obstacle is positioned closer to the landing perch. (*f*) Impulse angles increase during each flight as the bird accelerates after take-off and brakes before landing. Impulse angles near the obstacle also increase as the obstacle is positioned closer to the landing perch. (*g*) Stroke plane angles similarly increase over the course of each flight. (*h*) Wingbeat lift-to-drag ratios exhibit larger standard deviations, but typically more drag is used during flights over the obstacle and the subsequent landings.

separate tau functions—τ_{OB}, the perceived time-to-collision with the obstacle, and τ_{LD}, the perceived time-to-collision with the landing perch (see Material and methods). Compared with wingbeat accelerations directed towards or away from the obstacle (figure 5*e*), we find that accelerations directed towards the landing perch show a much stronger dependence on tau (figure 5*f*). This suggests that the birds' main objective in reorienting forces is to reach the landing perch. Meanwhile, their wingbeat impulses are timed to maintain a margin roughly equivalent to the
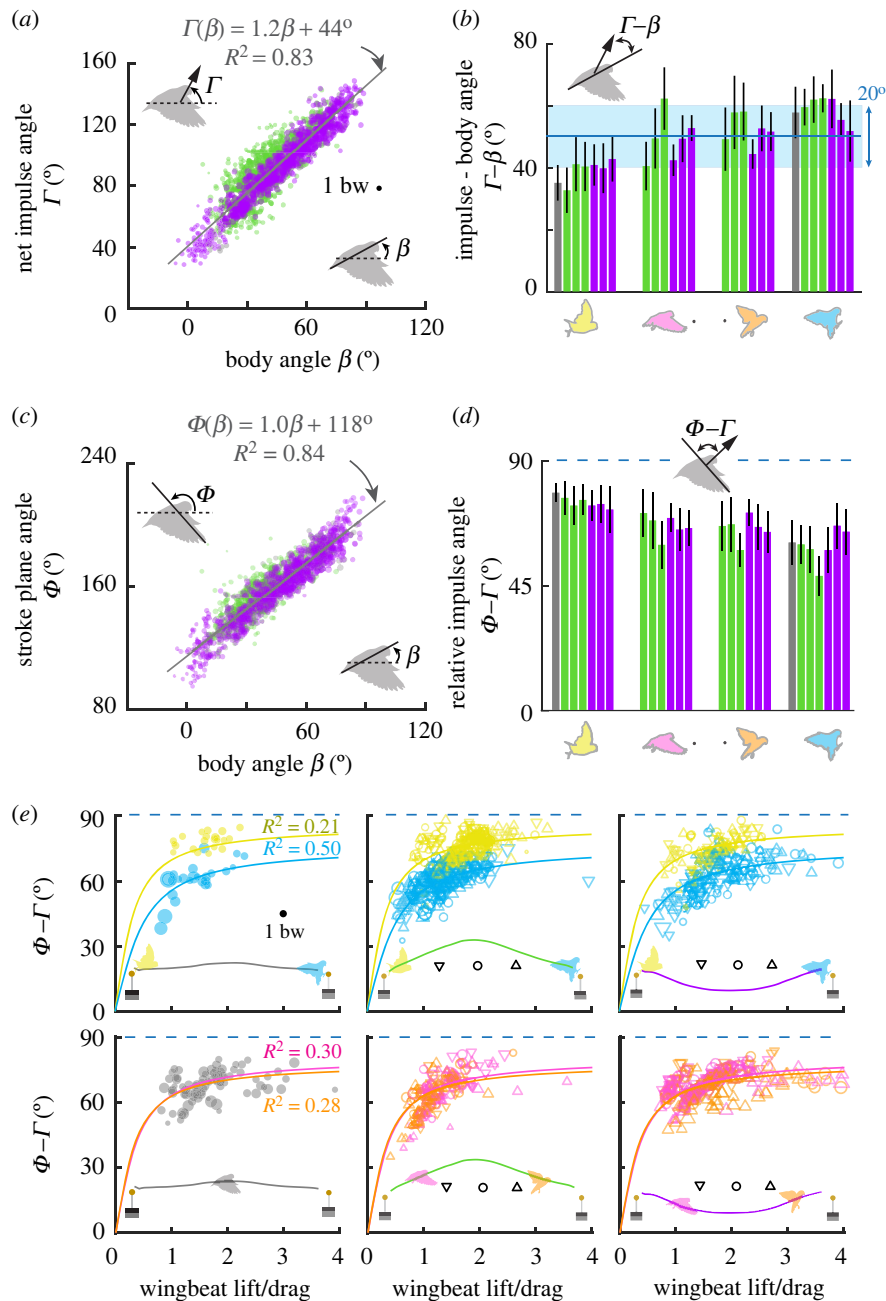
Figure 4. Birds direct aerodynamic force over a wide range of angles by combining body and stroke plane reorientation with variable lift-to-drag ratios. (a) Net wingbeat impulse angle Γ increases with body angle β, but the same net impulse direction can be achieved by body angles that diverge up to approximately 30°. Dots represent wingbeat averages (instantaneous force directions show even greater variance, figure 1c) and dot areas scale with wingbeat impulse magnitude (black dot = 1 bodyweight impulse; grey = baseline, green = flights over the obstacle, purple = flights under the obstacle). (b) Average wingbeat impulse directions vary with respect to the body frame more than the approximately 20° range previously reported for turning flight [6,10] (blue horizontal line shows average $\Gamma-\beta$, shaded region shows previously reported 20° range). Bars show mean ± s.d. for each variation (from left to right): baseline (if applicable), over 25/40/55 cm, under 25/40/55 cm. Wingbeats are categorized based on the bird's horizontal proximity to the perches or obstacle (take-off, landing = within 15 cm of the perch, before/after obstacle = within 10 cm of the string). (c) By pitching their bodies, parrotlets also pitch their stroke plane Φ, which remains at a relatively fixed offset with respect to their body axis ($\Phi-\beta=118°$, on average). For a and c, grey lines show the best-fit linear functions for $\Phi(\beta)$ and $\Gamma(\beta)$. (d) The stroke plane angle largely determines the net impulse angle (electronic supplementary material, figure S4), as shown here by the relative impulse angles (stroke plane angle Φ – net impulse angle Γ), which remain fairly consistent within each wingbeat type for a given flight variation. However, the relative impulse angles decrease towards landing, particularly for horizontal flights and flights over the obstacle, with the far obstacle corresponding with the smallest relative impulse angle. In contrast to helicopter rotors, the relative impulse angles are considerably less than 90° (blue dashed line, also shown in e), because birds generate and use stroke-averaged (net) drag. (e) Aerodynamic thrust vectoring adjustments can be achieved through variable lift-to-drag ratios, which result in large vector redirections for $\overline{L/D} \lesssim 2$. Wingbeats with more drag tended to have smaller relative impulse angles. During flights over an obstacle, take-off impulse tended to be oriented more perpendicular to the stroke plane while landing impulse tended towards smaller angles. Colours show wingbeat type (take-off = yellow, before obstacle = pink, after obstacle = orange, landing = blue, other wingbeats = grey). Symbols show distance variation (down triangle = 25 cm, circle = 40 cm, up triangle = 55 cm). Size of symbols correspond to relative impulse magnitude (black symbols show 1 bodyweight impulse). For each flight phase, an arctan function is fitted to the same-coloured data points (coefficients in electronic supplementary material, Table S3).

visuomotor delay range reported for pigeons [31] and dunlin [32], 30–70 ms, or about 0.6–1.5 parrotlet wingbeats (figure 5e,f). Spatially, this margin roughly corresponds to the distance needed for the wings to clear the obstacle when flying under it and for outstretched feet to reach the goal perch during landing, aiding flight safety.
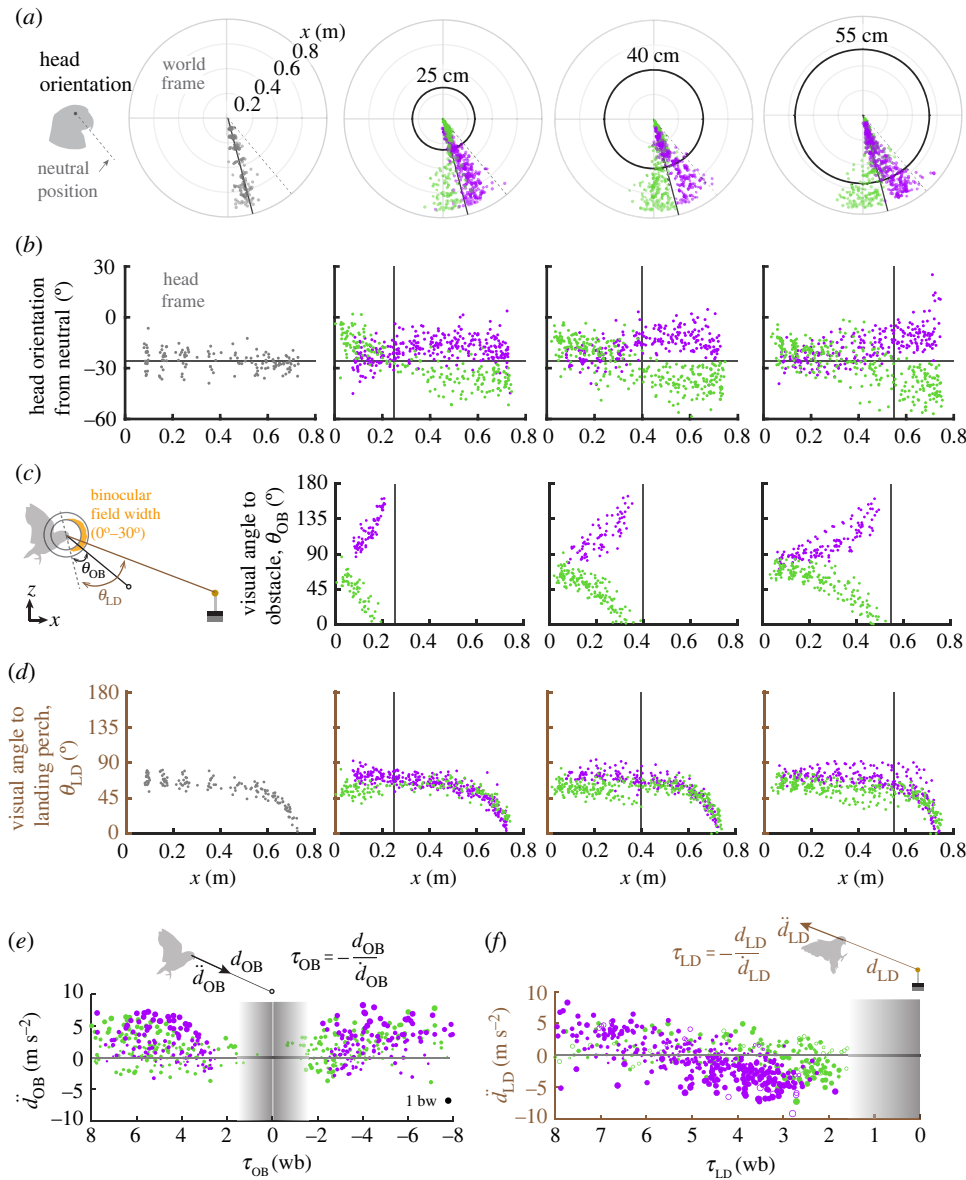
Figure 5. Birds use visual control to guide their landings while avoiding collisions with intervening obstacles. (*a*) The birds tilt their heads more downwards when flying over (green) an obstacle and more upwards when flying under (purple). Each dot shows the bird's head orientation, defined by a line from the bird's eye to tip of its beak, in the world frame during a downstroke. Black circles show obstacle positions, the dark grey radial lines show the average head orientation during baseline flights, and the thin dashed lines show the neutral (perched) head orientation from the inset for reference. (*b*) Head orientations from (*a*) are shown with respect to the neutral (perching) orientation. Grey horizontal lines show the average head orientation during baseline flights and vertical lines show obstacle positions. (*c*) These head orientation adjustments enable the birds to keep the obstacle in their approximately 180° field of view until they fly past it, as shown by the angle between their line-of-sight to the obstacle and their head orientation, θ_{OB}. (*d*) Meanwhile, the landing perch remains within their field-of-view for the duration of each flight. The angle between their line-of-sight to the landing perch and their head orientation (θ_{LD}) exhibits more variance during wingbeats before passing an obstacle compared with after. (*e*,*f*) Birds can visually estimate their time-to-collision with the obstacle τ_{OB} and landing perch τ_{LD} based on their distance from the obstacle d_{OB} and perch d_{LD}, and the time rate-of-change of that distance. (*e*) Wingbeat accelerations directed towards an obstacle $\ddot{d}_{OB}$ tend to decrease as the perceived time-to-collision τ_{OB} approaches 0 (τ_{OB} becomes negative when the bird flies away from the obstacle). (*f*) Wingbeat accelerations towards the landing perch $\ddot{d}_{LD}$ show a much stronger negative trend, with braking forces increasing as τ_{LD} decreases. Wingbeats from before a bird passes an obstacle are shown as open circles. In (*e*) and (*f*), grey shaded regions indicate the typical visuomotor delay for birds, 30–70 ms [28], or about 0.6–1.5 wingbeats. Parrotlets may avoid large wingbeats in this region to limit their risk of collision. Dot areas scale with the total wingbeat impulse (black dot in *e* corresponds to 1 bodyweight impulse).

3. Discussion

3.1. Visually guided force vectoring

The direct force and kinematic measurements from the parrotlets' perch-to-perch flights reveal how birds can both avoid and control collisions by harnessing visually guided force vectoring. A control scheme for foraging flights is outlined in figure 6 based on the observed behaviours and measured forces in this study. Each foraging flight begins

after a bird eyes the goal perch, identifies any obstacles, and then selects a suitable flight path. The birds initiate their strategy for flying over or under the obstacle by selecting a distinct angle to transfer impulse to the take-off perch (figures 2*b* and 6*b*). As they transition from the ground to air, they use both lift and drag for weight support and lift for forward thrust. Recently, we showed for obstacle-free horizontal flights that birds repurpose drag to support half of their bodyweight during take-off and lift to provide up to a quarter
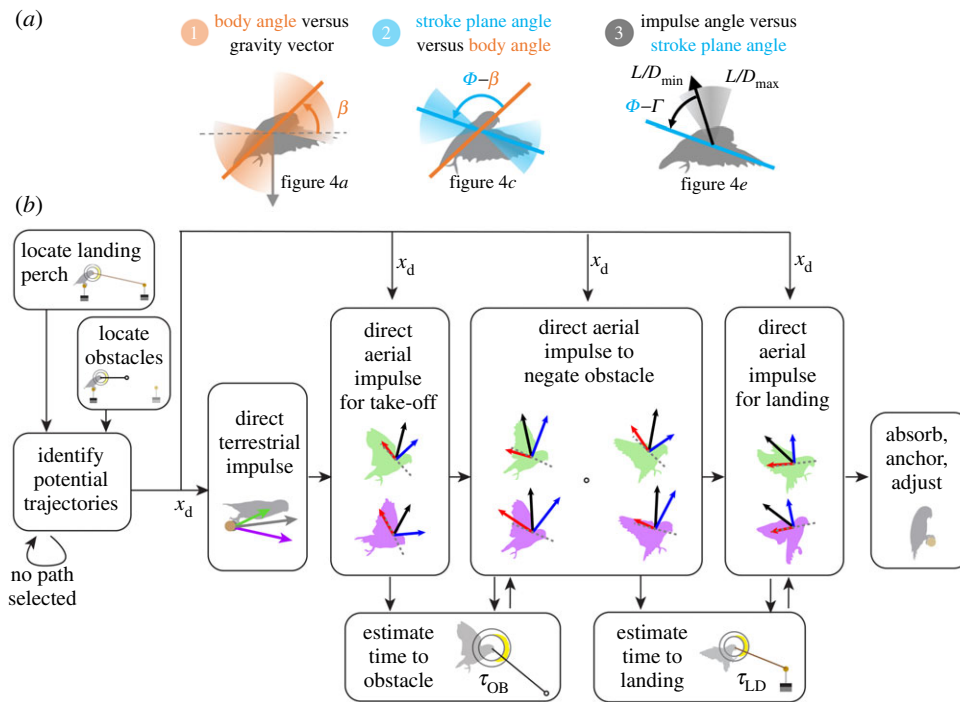
Figure 6. Informed by visual cues, birds use terrestrial and aerial force vectoring to avoid collisions with obstacles and perform controlled collisions for landing. (*a*) Birds perform aerodynamic force vectoring by adjusting (1) their body angle β in the global frame across a range of 101° (figure 4*a*), (2) their stroke plane angle Φ relative to their body angle across a range of 55° (figure 4*c*), and (3) lift-to-drag ratios to rotate their net wingbeat impulse vector relative to the stroke plane across a range of 53° (figure 4*e*). Diagrams show measured angle ranges for all wingbeats with an impulse greater than 90% bodyweight. These three key mechanisms enable birds to direct aerial impulse based on visual cues, as outlined in (*b*), a hypothesized control scheme for foraging flights based on quantified behaviour. After visually locating the landing perch and any intervening obstacles, birds select a desired trajectory x_d to begin their flight. The decision to fly over (green) or under (purple) an obstacle largely determines how the birds direct their terrestrial impulse during take-off. The intended flight path also determines how lift (blue arrows) and drag (red arrows) are oriented during initial wingbeats. Based on their current position and velocity, the birds can visually estimate how much time they have before a collision with the obstacle would occur (τ_{OB}). They must then direct aerial impulse by adjusting their stroke kinematics to track their desired flight path x_d while maintaining a safe margin from the obstacle. After passing the obstacle, the birds need only consider their time-to-collision with the landing perch (τ_{LD}). They can then redirect lift and drag to direct aerial impulse for a controlled collision. Upon touchdown, the legs absorb most of their remaining kinetic energy while the feet and claws secure their grasp on the perch [33].

of the horizontal braking forces during landing [34]. Here we find that they continue to adapt drag and lift for manoeuvring flight by rotating drag and lift more forwards for flying under an obstacle compared with flying over (figures 3*a–d* and 6). In fact, compared with level flights, birds repurpose drag and lift to an even greater extent for take-off and landing, supporting up to 71% bodyweight with drag on take-off and up to 40% of horizontal braking force with lift upon landing (electronic supplementary material, table S4).

Previous studies have shown how birds rely on visual control to manoeuvre [35–38], avoid obstacles [39] and land [30,33,40]. Accordingly, we found most birds showed increased head motion (side-to-side or fore-and-aft) prior to take-off, presumably to identify obstacles and viable flight paths to the goal perch. Based on the differences in take-off impulse direction with and without obstacles (figure 2*a*), they select their flight path prior to pushing off, indicating that they must be using visual cues even before they take off. As they continue towards the goal perch, the birds incorporate more visual cues to inform their aerodynamic force vectoring (figure 6). For all obstacle flights, they maintain a view of both the obstacle and the landing perch before passing the obstacle (figure 5*c,d*). This enables them to maintain a safe margin from the obstacle (figure 5*e*) until passing it, after which they direct their gaze more consistently towards the landing perch (figure 5*d*). The wingbeat pauses that often

occur during flights with no obstacle or flights over an obstacle (figure 1*c*; electronic supplementary material, table S5) may be used for flight control. The brief pause can enable the birds to take in more visual information that flapping wings may partially obscure, not unlike how lovebirds time their head saccades to limit wingbeat occlusion of their visual field [28]. After the brief pause, the parrotlets can adjust their wingbeats to the perceived time-to-collision as needed. The increased weight support needed for manoeuvring under an obstacle (figures 2*a* and 3*e*) may be prohibitive for the birds to incorporate pauses mid-flight, but they can make timing adjustments just after take-off or before landing instead (e.g. figure 1*c*). Once their visually estimated time to the landing perch falls within a few wingbeats, the birds begin a more stereotyped braking process for landing [33] (figure 5*f*). This process may be easier when ascending from flying under an obstacle, not only because gravity aids in the deceleration process, but also because lift can provide up to 40% of the total horizontal braking force. As a result, less drag is required to slow down compared with landing wingbeats after flying over obstacles (figure 3*b–d*). This may also explain the larger temporal and spatial margin between their final wingbeats and the landing perch for flights under an obstacle (figure 5*f*). The flights conclude as the birds touch down, at which point their legs absorb the remaining energy and their feet and claws secure their grasp on the landing perch [33].

3.2. Force vectoring versatility

Based on their intended path and updated visual cues (figure 5), the parrotlets can adjust the direction of their aerial impulses by combining stroke plane angle modulation (figure 4c) with aerodynamic force vectoring relative to their stroke plane (figure 4e). In doing so, the net wingbeat force vectors necessarily remain—on average—pointing upwards to support bodyweight (figure 2a), but their orientation relative to the body changes quite substantially beat to beat to manoeuvre (figure 4a,b). The birds achieve a range of stroke-averaged impulse angles over 100° in the global reference frame (figure 4c) through extremely rapid angular pitching rates that modulate their stroke plane angles at hundreds of degrees per second (electronic supplementary material, figure S5). Manoeuvring via stroke plane angle adjustments is similar to the force vectoring mechanism used by helicopters, as previous animal flight studies have suggested [6,10,20]. However, the parrotlets' mechanism differs in two critical ways. First, the net aerodynamic impulse never acts orthogonally to the stroke plane (figure 4d,e), because the birds harness stroke-averaged drag (figure 3a–d). Variability in their use of wingbeat kinematics and lift-to-drag ratios leads to the second key difference: the net force angle that we directly measured is not as fixed relative to either the body (figure 4b) or stroke plane angle (figure 4d) as Muijres *et al.* [6] found for flies making extreme banked turns (measured with a robot), or as Ros *et al.* [10] computed for turning pigeons (via inverse dynamics). These studies reported variations in force direction relative to body orientation of only approximately 20°. Compared with turning, greater changes in force direction relative to the body may be needed to adjust flight paths in the vertical direction and for landing manoeuvres. Indeed the average direction of the net wingbeat impulse relative to the stroke plane that we measured *in vivo* typically spans a range of approximately 30° across flight phases (figure 4d) but can range up to approximately 50° for individual wingbeats (figure 4e). The full range of impulse angles achieved by parrotlets is thus more similar to that of supermanoeuvrable fighter aircraft that thrust vector their jet beyond the aerodynamic limits of their fixed wings to perform vertical/short take-offs and landings [41]. By contrast, birds achieve this range aerodynamically by repurposing their wings' elevated lift and drag unconventionally.

The ability to adjust both stroke plane angles and wingbeat lift-to-drag ratios grants parrotlets exceptional versatility in their force vectoring capabilities (figure 4). While these two mechanisms often act in conjunction, they can also be used independently; if a bird is more constrained in its ability to modulate stroke plane angle relative to its body axis, it can modulate net lift and drag through angle-of-attack adjustments to redirect forces relative to its stroke plane, and vice versa. Without the ability to adjust force direction independent of body angle, the birds would need to rely on slower acceleration and deceleration rates, or they would need to pitch further forwards or backwards to accelerate and decelerate. Large changes in body pitch may be detrimental for stability and for maintaining visual control during flight manoeuvres.

3.3. Drag facilitates avian take-off and manoeuvring

The versatile force vectoring that parrotlets exhibit during their short, foraging flights can provide insight into how birds evolved their ability to hop and fly in arboreal environments. Although drag requires energy expenditure that lift does not, it substantially augments the total aerodynamic force when lift alone may not be sufficient [34]. This is advantageous when elevated drag is harnessed for just a few wingbeats, because the elevated aerodynamic power (drag × wing velocity) only constitutes a small energetic penalty (elevated power × brief time period), especially compared with the total energy expenditure over the entire flight duration involving numerous wingbeats. The elevated aerodynamic power can be sustained by bird muscles during a few wingbeats, because they have the capacity to deliver high burst power [42]. Critically, supporting weight with drag requires much less muscle power when drag only has to support a fraction of bodyweight. We previously showed how even limited weight support from a single proto-wingbeat could have increased the long-jump range of foraging arboreal dinosaurs [22]. Drag forces would have been sufficient to supply these aerodynamic forces and significantly extend long-jump range, especially for avian precursors with limited lift-generating capabilities [34]. Here, we find that drag can contribute up to 70% of bodyweight support during flights requiring obstacle negotiation. The ability to generate drag would have also contributed towards redirecting aerodynamic force (relative to the global frame), which is critical for making foraging flights. This insight explains how, despite their minimal lift and high drag, proto-wings could have furnished the origin of bird flight [43] from the first extended long jump [22] and aerodynamic take-off [34] towards foraging flights. According to the ontogenetic-transitional wing hypothesis [20], early fliers moved their proto-wings through a fundamental stroke plane similar to that of juvenile ground birds. These ground birds flap their transitional wings through a stroke plane that remains approximately fixed with respect to gravity during descending flight and wing-assisted inclined running [20]. However, compared with descending flight or inclined running, arboreal foraging flights require a much larger range of force directions for birds to accelerate after take-off and brake before landing. In order to increase their range of force directions and improve aerodynamic control, avian precursors would have needed to expand their range of stroke plane angles and ability to adjust wing orientations, which adds greater complexity to wing biomechanics and flight control [10], but also greatly enhances manoeuvrability. Thus, as avian precursors improved their flight capabilities, they probably increased both the magnitude of aerodynamic force generated by their wings and their range of stroke plane angles and net force orientations—by using lift and drag interchangeably. With greater flexibility in their ability to redirect aerodynamic forces, the first birds could better direct forces to fly further and with more control. Guided by time-to-collision visual cues they then could have transitioned to fly up or down to deftly navigate around obstacles and reach previously unattainable foraging locations effectively.

4. Material and methods

4.1. Experimental design

In order to evaluate how birds navigate around horizontal obstacles during short, foraging flights, we studied perch-to-perch flights made by five Pacific parrotlets (*F. coelestis*; 30.7 ± 26 g) inside of an AFP. We chose white string as the obstacle for three main reasons: (i) it is clearly visible against the black

background formed by the force plates of the AFP, (ii) it was non-rigid so birds would not perch on it and would not be harmed if they contacted it, and (iii) it was thin enough to avoid introducing significant interference with airflow inside of the AFP generated by the birds' wingbeats. We tested 10 variations: one baseline with no obstacle; three with a single string hung across the width of the AFP at eye-level with a parrotlet resting on the take-off perch; three where additional strings were added below the original (to block off the option to fly under the obstacle); and three where additional strings were added above the original (to block off the option to fly over the obstacle). After testing the baseline case, we tested all single-string variations first to avoid biasing the parrotlets' selected strategy for flying over versus under the obstacles. The obstacles were positioned halfway between the perches (40 cm from the take-off perch), 25 cm from the take-off perch, and then 55 cm from the take-off perch. For each variation, we recorded four flights per bird for five birds. Flights in which birds did not fly towards the landing perch were labelled as outliers by an impartial third party based solely on videos. Five outlier flights were omitted from our analysis, except for evaluating whether there was a preferred flight strategy. The preferred strategy (i.e. flying over or under the obstacle) turned out to be specific to each individual (electronic supplementary material, table S1). Budgerigars have similarly exhibited individual biases in flying left or right around a barrier [44]. To determine how the birds negotiated horizontal obstacles mechanistically, we pooled our data from the single string variations with the remaining obstacle variations. We thus report mean ± s.d. based on $N = 5$ birds, $n_{baseline} = 20$ flights (4 per bird), $n_{over,25\,cm} = 22$ flights (4–6 per bird), $n_{over,40\,cm} = 29$ flights (4–8 per bird), $n_{over,55\,cm} = 29$ flights (3–8 per bird), $n_{under,25\,cm} = 36$ flights (4–8 per bird), $n_{under,40\,cm} = 28$ flights (3–8 per bird), $n_{under,55\,cm} = 28$ flights (4–8 per bird).

The birds were trained using habituation and positive reinforcement (with millet seed rewards) to fly inside of the AFP with no obstacle present. Once the birds flew consistently on cue (when the trainer pointed a finger or target stick at the goal perch), we recorded the baseline flights and then tested the single string variations. When additional strings were added above and below the single string, another round of habituation and positive reinforcement training preceded the experimental recordings.

4.2. Force measurements

Net instantaneous vertical and horizontal aerodynamic forces were measured using a two-dimensional AFP (figure 1a). The floor, ceiling and front and back walls of the AFP ($100 \times 100 \times 60$ cm; length × height × width) are made of carbon fibre sandwich panels, each attached in a statically determined manner to three Nano 43 sensors (six-axis, SI-9-9.125 calibration; ATI Industrial Automation) sampling at 2000 Hz (100× the parrotlets' wingbeat frequency of 20 Hz) with a resolution of 2 mN (less than 1% the parrotlets' average bodyweight of 363 mN). The side walls are formed from clear acrylic panels. Take-off and landing forces were measured using instrumented perches that extended through the side walls of the AFP. Further details of this set-up are published elsewhere [34]. All force measurements were filtered using an eighth-order Butterworth filter with a cut-off frequency of 80 Hz for the plates and 40 Hz for the perches, which had a lower natural frequency (greater than 44 Hz) than the force plates (greater than 92 Hz). Integrated forces matched expected net impulse values (electronic supplementary material, table S6) based on the conservation of momentum [34].

As detailed in our previous work [32], we determined force contributions from the parrotlets' body and tail to be negligible during slow flight (less than 1% bodyweight based on a drag coefficient of 0.4), because force contributions scale with velocity^2 ×

area. The body and tail have a much slower velocity (1.7 m s^{-1} average across all variations) compared with the velocity at the radius of gyration of the flapping wings (4.2 m s^{-1} average), and their total surface area is only about a quarter of the area of the wings (0.002 m^2 versus 0.008 m^2). We therefore attribute all measured aerodynamic forces to the parrotlets' flapping wings (20 Hz wingbeat frequency, 22.0 ± 1.5 cm wingspan).

4.3. Kinematics

Body and wingbeat kinematics were captured using five high-speed cameras (three Phantom Miro M310 s, one R-311, and one LC310, 1280×800 resolution, 1000 fps), synchronized with each other and the force sensors. The cameras were calibrated using DLT software [45] with an average DLT error less than 1%. Points on the birds' eye and tail were digitized throughout the flight, and on the birds' shoulder and wingtip at the start and end of each downstroke (see electronic supplementary materials for details).

The eye and tip of the beak were manually tracked during mid-downstroke to recover head orientation, which we defined as the angle of the line connecting these two points. To determine whether the landing perch and obstacle were in the bird's field-of-view, we measured the angle of a line drawn from the bird's eye to the obstacle or perch relative to the bird's head orientation (figure 4b,c).

Time-to-collision with the obstacle, τ_{OB} (figure 5e), was calculated as the distance between the bird's eye and obstacle divided by the time rate of change of that distance. Time-to-collision with the landing perch, τ_{LD} (figure 5f), was calculated as the distance between the instantaneous position of the bird's eye and the eye position when its feet made contact with the landing perch divided by the time rate of change of that distance.

4.4. Calculating lift and drag

To determine lift and drag, we decompose the measured aerodynamic forces into components that act orthogonal to the bird's wing velocity (lift) and antiparallel to the wing velocity (drag). To recover the bird's instantaneous wing velocity based on our kinematic measurements from the start and end of each stroke, we model stroke angle ϕ (electronic supplementary material, figure S6A) as a sinusoidal function, $\phi = A/2 \cos(2\pi f(t - t_o)) + \phi_o$, where A is the measured stroke amplitude, f is stroke frequency, t is time with phase offset t_o, and ϕ_o is stroke angle offset because the wingbeats were not symmetric about the horizontal plane. Stroke amplitude A and stroke angle offset ϕ_o are based on the location of the bird's wingtip and shoulder at the start and end of each downstroke. We also use the bird's wingtip position at the start and end of downstroke to determine average stroke plane angle Φ_o. The bird's wing trajectory deviates from this angle up to a maximum stroke deviation angle of δ_o, so we model the stroke plane angle as $\Phi = \Phi_o + \delta_o (\cos(2\pi f t) - 1)$ during accelerating wingbeats (stroke plane pitched forwards, electronic supplementary material, figure S6B), and as $\Phi = \Phi_o - \delta_o (\sin(2\pi f t) - 1)$ during braking wingbeats (stroke plane pitched backwards, electronic supplementary material, figure S6C). Combining these modelled kinematics, we can derive the three-dimensional wing velocity and radius vectors (see electronic supplementary material for more details) to calculate lift and drag as in [34]. Comparing these calculations based on modelled wing kinematics with calculations based on our fully resolved wingbeat kinematics during the baseline flights (electronic supplementary material, figure S6), we find reasonable agreement for lift and drag impulse magnitudes and directions during a take-off, mid-flight and landing wingbeat (electronic supplementary material, table S2).

Lift and drag were averaged separately for each wingbeat to calculate their contributions to weight support and braking (electronic supplementary material, table S4), and to calculate lift-to-drag ratios (figures 3h and 4e). This averaging method

is more robust to kinematics modelling errors and noise in the data, but is non-conservative; wingbeat-averaged lift and wingbeat-averaged drag do not necessarily sum up to wingbeat-averaged net force. For a more intuitive snapshot of lift and drag contributions during different wingbeats, we show instantaneous force vectors in figure 3a–d, for which lift and drag do sum to net force. To select the representative wingbeats from which these mid-downstroke vectors were extracted, we identified wingbeats with drag or lift contributions that were most similar to the contributions listed in electronic supplementary material, table S4.

References

1. Witter MS, Cuthill IC. 1993 The ecological costs of avian fat storage. *Phil. Trans. R. Soc. Lond. B* **340**, 73–92. (doi:10.1098/rstb.1993.0050)

2. Williams CD, Biewener AA. 2015 Pigeons trade efficiency for stability in response to level of challenge during confined flight. *Proc. Natl Acad. Sci. USA* **112**, 3392–3396. (doi:10.1073/pnas.1407298112)

3. Henningsson P. 2021 Flying through gaps: how does a bird deal with the problem and what costs are there? *R. Soc. Open Sci.* **8**, 211072. (doi:10.1098/rsos.211072)

4. Robinson SK, Holmes RT. 1982 Foraging behavior of forest birds: the relationships among search tactics, diet, and habitat structure. *Ecology* **63**, 1918–1931. (doi:10.2307/1940130)

5. Tobalske BW. 2007 Biomechanics of bird flight. *J. Exp. Biol.* **210**, 3135–3146. (doi:10.1242/jeb.000273)

6. Muijres FT, Elzinga MJ, Melis JM, Dickinson MH. 2014 Flies evade looming targets by executing rapid visually directed banked turns. *Science* **344**, 172–177. (doi:10.1126/science.1248955)

7. Zeyghami S, Babu N, Dong H. 2016 Cicada (*Tibicen linnei*) steers by force vectoring. *Theor. Appl. Mech. Lett.* **6**, 107–111. (doi:10.1016/j.taml.2015.12.006)

8. Fry SN, Sayaman R, Dickinson MH. 2003 The aerodynamics of free-flight maneuvers in *Drosophila*. *Science* **300**, 495–498. (doi:10.1126/science.1081944)

9. Iriarte-Díaz J, Swartz SM. 2008 Kinematics of slow turn maneuvering in the fruit bat *Cynopterus brachyotis*. *J. Exp. Biol.* **211**, 3478–3489. (doi:10.1242/jeb.017590)

10. Ros IG, Bassman LC, Badger MA, Pierson AN, Biewener AA. 2011 Pigeons steer like helicopters and generate down- and upstroke lift during low speed turns. *Proc. Natl Acad. Sci. USA* **108**, 19 990–19 995. (doi:10.1073/pnas.1107519108)

11. Hedrick TL, Usherwood JR, Biewener AA. 2007 Low speed maneuvering flight of the rose-breasted cockatoo (*Eolophus roseicapillus*). II. Inertial and aerodynamic reorientation. *J. Exp. Biol.* **210**, 1912–1924. (doi:10.1242/jeb.002063)

12. Dudley R. 2002 Mechanisms and implications of animal flight maneuverability. *Integr. Comp. Biol.* **42**, 135–140. (doi:10.1093/icb/42.1.135)

13. Biewener A, Patek S. 2018 *Animal locomotion*. Oxford, UK: Oxford University Press.

14. Hsu S-J, Thakur N, Cheng B. 2019 Speed control and force-vectoring of bluebottle flies in a magnetically levitated flight mill. *J. Exp. Biol.* **222**, jeb187211. (doi:10.1242/jeb.187211)

15. Leishman JG. 2006 *Principles of helicopter aerodynamics*, 2nd edn. Cambridge, UK: Cambridge University Press.

16. Alexander DE. 1986 Wind tunnel studies of turns by flying dragonflies. *J. Exp. Biol.* **122**, 81–98. (doi:10.1242/jeb.122.1.81)

17. Warrick DR. 1998 The turning- and linear-maneuvering performance of birds: the cost of efficiency for coursing insectivores. *Can. J. Zool.* **76**, 1063–1079. (doi:10.1139/z98-044)

18. Cheng B, Tobalske BW, Powers DR, Hedrick TL, Wethington SM, Chiu GTC, Deng X. 2016 Flight mechanics and control of escape manoeuvres in hummingbirds. I. Flight kinematics. *J. Exp. Biol.* **219**, 3518–3531. (doi:10.1242/jeb.137539)

19. Altshuler DL, Quicazán-Rubio EM, Segre PS, Middleton KM. 2012 Wingbeat kinematics and motor control of yaw turns in Anna's hummingbirds (*Calypte anna*). *J. Exp. Biol.* **215**, 4070–4084. (doi:10.1242/jeb.075044)

20. Dial KP, Jackson BE, Segre P. 2008 A fundamental avian wing-stroke provides a new perspective on the evolution of flight. *Nature* **451**, 985–989. (doi:10.1038/nature06517)

21. Berg AM, Biewener AA. 2010 Wing and body kinematics of takeoff and landing flight in the pigeon (*Columba livia*). *J. Exp. Biol.* **213**, 1651–1658. (doi:10.1242/jeb.038109)

22. Chin DD, Lentink D. 2017 How birds direct impulse to minimize the energetic cost of foraging flight. *Sci. Adv.* **3**, e1603041. (doi:10.1126/sciadv.1603041)

23. Carruthers AC, Thomas ALR, Taylor GK. 2007 Automatic aeroelastic devices in the wings of a steppe eagle *Aquila nipalensis*. *J. Exp. Biol.* **210**, 4136–4149. (doi:10.1242/jeb.011197)

24. Tomotani BM, Muijres FT. 2019 A songbird compensates for wing molt during escape flights by reducing the molt gap and increasing angle of attack. *J. Exp. Biol.* **222**, jeb195396. (doi:10.1242/jeb.195396)

25. Forshaw J. 2010 *Parrots of the world*. Princeton, NJ: Princeton University Press.

26. Cheng B, Tobalske BW, Powers DR, Hedrick TL, Wang Y, Wethington SM, Chiu GT, Deng X. 2016 Flight mechanics and control of escape manoeuvres in hummingbirds. II. Aerodynamic force production, flight control and performance limitations. *J. Exp. Biol.* **219**, 3532–3543. (doi:10.1242/jeb.137570)

27. Ellington CP. 1984 The aerodynamics of hovering insect flight. VI. Lift and power requirements. *Phil. Trans. R. Soc. Lond. B* **305**, 145–181. (doi:10.1098/rstb.1984.0054)

28. Kress D, van Bokhorst E, Lentink D, Wylie D. 2015 Correction: how lovebirds maneuver rapidly using super-fast head saccades and image feature stabilization. *PLoS ONE* **10**, e0129287. (doi:10.1371/journal.pone.0129287)

29. Demery ZP, Chappell J, Martin GR. 2011 Vision, touch and object manipulation in Senegal parrots *Poicephalus senegalus*. *Proc. R. Soc. B* **278**, 3687–3693. (doi:10.1098/rspb.2011.0374)

30. Lee D, Davies M, Green P. 1993 Visual control of velocity of approach by pigeons when landing. *J. Exp. Biol.* **180**, 85–104. (doi:10.1242/jeb.180.1.85)

31. Stitt CL, Hoffman HS, Marsh RR, Schwartz GM. 1976 Modification of the pigeon's visual startle reaction by the sensory environment. *J. Comp. Physiol. Psychol.* **90**, 601–619. (doi:10.1037/h0077222)

32. Potts WK. 1984 The chorus-line hypothesis of manoeuvre coordination in avian flocks. *Nature* **309**, 344–345. (doi:10.1038/309344a0)

33. Roderick WRT, Chin DD, Cutkosky MR, Lentink D. 2019 Birds land reliably on complex surfaces by

adapting their foot-surface interactions upon contact. *Elife* **8**, 1–23. (doi:10.7554/elife.46415)

34. Chin DD, Lentink D. 2019 Birds repurpose the role of drag and lift to take off and land. *Nat. Commun.* **10**, 5354. (doi:10.1038/s41467-019-13347-3)

35. Ros IG, Bhagavatula PS, Lin HT, Biewener AA. 2017 Rules to fly by: pigeons navigating horizontal obstacles limit steering by selecting gaps most aligned to their flight direction. *Interface Focus* **7**, 20160093. (doi:10.1098/rsfs.2016.0093)

36. Lin H-T, Ros IG, Biewener AA. 2014 Through the eyes of a bird: modelling visually guided obstacle flight. *J. R. Soc. Interface* **11**, 20140239. (doi:10.1098/rsif.2014.0239)

37. Schiffner I, Srinivasan MV. 2015 Direct evidence for vision-based control of flight speed in budgerigars. *Sci. Rep.* **5**, 10992. (doi:10.1038/srep10992)

38. Dakin R, Fellows TK, Altshuler DL. 2016 Visual guidance of forward flight in hummingbirds reveals control based on image features instead of pattern velocity. *Proc. Natl Acad. Sci. USA* **113**, 8849–8854. (doi:10.1073/pnas.1603221113)

39. Karmaker D, Groening J, Wilson M, Schiffner I, Srinivasan MV. 2020 Budgerigars adopt robust, but idiosyncratic flight paths. *Sci. Rep.* **10**, 1–12. (doi:10.1038/s41598-020-59013-3)

40. Bhagavatula P, Claudianos C, Ibbotson M, Srinivasan M. 2009 Edge detection in landing budgerigars (*Melopsittacus undulatus*). *PLoS ONE* **4**, e7301. (doi:10.1371/journal.pone.0007301)

41. Gal-Or B. 2013 *Vectored propulsion, supermaneuverability and robot aircraft*. New York, NY: Springer.

42. Jackson BE, Dial KP. 2011 Scaling of mechanical power output during burst escape flight in the Corvidae. *J. Exp. Biol.* **214**, 452–461. (doi:10.1242/jeb.046789)

43. Xu X, Zhou Z, Dudley R, Mackem S, Chuong C, Erickson GM, Varricchio DJ. 2014 An integrative approach to understanding bird origins. *Science* **346**, 1253293. (doi:10.1126/science.1253293)

44. Bhagavatula PS, Claudianos C, Ibbotson MR, Srinivasan MV. 2014 Behavioral lateralization and optimal route choice in flying budgerigars. *PLoS Comput. Biol.* **10**, e1003473. (doi:10.1371/journal.pcbi.1003473)

45. Hedrick TL. 2008 Software techniques for two- and three-dimensional kinematic measurements of biological and biomimetic systems. *Bioinspir. Biomim.* **3**, 034001. (doi:10.1088/1748-3182/3/3/034001)

46. Chin DD, Lentink D. 2022 Birds both avoid and control collisions by harnessing visually guided force vectoring. Figshare. (doi:10.6084/m9.figshare.c.6016857)